



Title	Solute atom mediated crystallization of amorphous alloys
Author(s)	Sato, Kazuhisa; Mori, Hirotarō
Citation	Materialia. 2023, 32, p. 101888
Version Type	VoR
URL	https://hdl.handle.net/11094/97369
rights	This article is licensed under a Creative Commons Attribution 4.0 International License.
Note	

The University of Osaka Institutional Knowledge Archive : OUKA

<https://ir.library.osaka-u.ac.jp/>

The University of Osaka



Full Length Article

Solute atom mediated crystallization of amorphous alloys

Kazuhisa Sato^{*}, Hirotarō Mori

Research Center for Ultra-High Voltage Electron Microscopy, Osaka University, 7-1 Mihogaoka, Ibaraki, 567-0047, Japan

ARTICLE INFO

Keywords:

Electronic excitation
Electron irradiation
Pd-Si
Amorphous alloy
Crystallization

ABSTRACT

We propose a new mechanism of crystallization of amorphous alloy which is mediated by additional solute atoms produced by electronic excitation. For a freestanding Pd-19at%Si amorphous alloy film, electron irradiation causes subtle structural change. By contrast, extensive crystallization of Pd-19at%Si amorphous alloy sandwiched by amorphous (a-) SiO_x films, i.e., a-SiO_x/a-Pd-Si/a-SiO_x, occurred by 75 keV and 200 keV electron irradiation. This crystallization was induced by irradiation not only at room temperature but also even at 90 K. It should be emphasized that the crystallization can be realized by 75 keV irradiation at 90 K via the electronic excitation; where both knock-on damage and a possible thermal crystallization can be excluded. A resultant product of the crystallization after electronic excitation (i.e., electron irradiation), hexagonal Pd₂Si, differs from that of thermal annealing (orthorhombic Pd₃Si). Evidence for decomposition of a-SiO_x by electronic excitation contributes essentially to the crystallization of the a-Pd-Si in the composite film has been obtained in this study. Supply of dissociated Si to the a-Pd-Si layer may cause instability of the amorphous phase, which serves as the trigger for the remarkable structural change; i.e., additional solute atom mediated crystallization.

1. Introduction

In general, amorphous materials are thermodynamically metastable and they transform to equilibrium phase(s), i.e., crystalline solids, with the assistance of thermal energy [1]. It is known in most cases crystallization proceeds towards stable phase(s) via several metastable phases [2]. Also it is known the thermal stability of amorphous phase was enhanced by increasing the number of constituent components, which contributed to the development of bulk metallic glasses [3]. If we confine ourselves to inorganic amorphous materials, the origin of crystallization is not limited to the thermal energy, but an ionization process can also induce crystallization. Such an athermal crystallization has been reported for oxide compounds [4], Al₂O₃ [5], Si [6], Ge [6,7], and SiGe [8]. In these studies, origin of the crystallization has been attributed to electronic excitation since the crystallization proceeds under irradiation conditions where knock-on atom displacement is absent. However, it is critical to discriminate whether the origin of the crystallization is purely ionization or includes thermal energy assistance as well.

The Pd-Si alloy system is a famous amorphous forming system by quenching from the melt [9]. In a normal heat treatment, Pd₃Si is formed via precipitation of several metastable phases [10]. On the other hand, Nagase et al. reported that Pd₂Si was formed by electron

irradiation at room temperature, mainly based on the experimental results of 200 keV-electron irradiation at 298 K [11]. The important point here is that the amorphous Pd-Si (hereafter, a-Pd-Si) was in contact with amorphous SiO_x (x~1.5, hereafter, a-SiO_x) in their work. A possible role of a-SiO_x upon crystallization is considered to be dissociation of the oxide induced by electron irradiation. Regarding this point, we have studied dissociation of a-SiO_x using photon irradiation and found that excitation of Si2p electrons followed by Auger decay of the core hole is responsible for the dissociation process [12,13]. The dominant valence state was Si³⁺ before photon irradiation, and then, Si⁴⁺ and Si⁰ markedly increased after photon irradiation [13]. Thus, it is presumed that the crystallization of a-Pd-Si could be directly related to the decomposition of a-SiO_x by electronic excitation.

In this study, we have made clear the effect of additional Si on the electron irradiation induced crystallization of a-Pd-Si alloy thin films using transmission electron microscopy (TEM) and electron diffraction. Based upon the results, proposed is a new mechanism of crystallization of amorphous alloys mediated by additional solute atoms.

^{*} Corresponding author.

E-mail address: sato@uhvem.osaka-u.ac.jp (K. Sato).

<https://doi.org/10.1016/j.mtla.2023.101888>

Received 28 July 2023; Accepted 2 September 2023

Available online 2 September 2023

2589-1529/© 2023 The Author(s). Published by Elsevier B.V. on behalf of Acta Materialia Inc. This is an open access article under the CC BY license (<http://creativecommons.org/licenses/by/4.0/>).

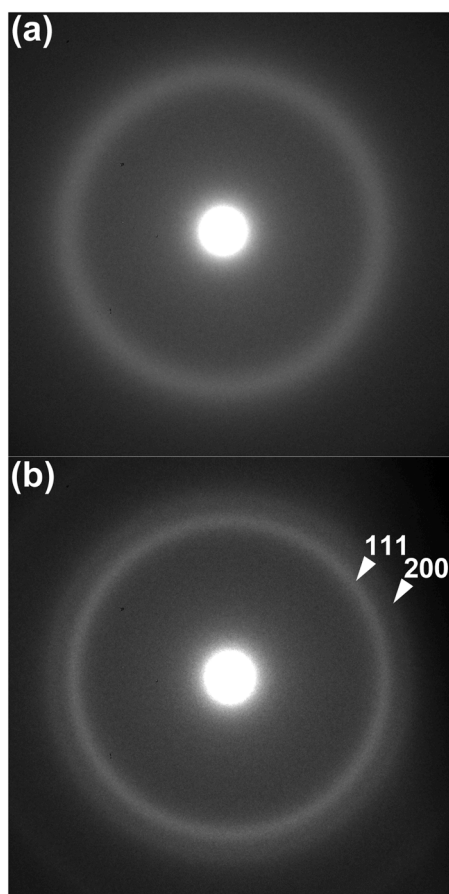


Fig. 1. SAED patterns of an a-Pd₈₁Si₁₉ alloy film. (a) as-deposited, (b) after 75 keV-electron irradiation at 298 K for 2.9 ks (total dose: 2.9×10^{27} e/m²).

2. Experimental procedures

2.1. Specimen preparation

Thin films of a-Pd-Si alloy were fabricated by the co-deposition of Pd and Si targets using dc magnetron sputtering. Two kinds of substrates, NaCl(001) cleaved in air and a-SiO_x thin films deposited onto NaCl substrates, were used in this study. The oxygen content, *x*, in the a-SiO_x film was approximately 1.5 as determined by the preceding study [14]. The substrate temperature was kept at room temperature during the sputtering. Sputtering was performed in high-purity Ar (99.999%) gas at a pressure of 8 Pa and a power of 100 W with a chamber base pressure of 6×10^{-6} Pa. The alloy composition of the sputtered films was Pd-19at% Si according to the elemental analyses (EDS, see Section 2.2). Specimens sputtered onto the a-SiO_x thin films on NaCl were further coated by a-SiO_x to prepare a-Pd-Si thin films sandwiched by a-SiO_x films (i.e., a-SiO_x/a-Pd-Si/a-SiO_x). The prepared thin films were then floated on distilled water and mounted onto copper grids for TEM observation (plan-view observation). Cross-sectional TEM specimens were prepared from the sandwiched films that had been in advance mounted on Si(111) wafers using a focused ion beam (FIB) instrument (Thermo Fisher Scientific Scios2 Dual Beam) (cross-sectional view observation). It is noted that in cross-sectional TEM observation, electron irradiation was carried out in the direction parallel to the a-SiO_x/a-Pd-Si interface. In Section 3, results obtained in the plan-view TEM observation and those in the cross-sectional TEM observation are shown in sequence.

2.2. Electron irradiation and TEM observation

The prepared thin films on copper grids were irradiated with 75 keV

and 200 keV electrons using TEMs (Hitachi H-7000 with a LaB₆ cathode and JEOL JEM-ARM200F with a Schottky field emission gun). The electron dose rate was estimated using a Faraday cage attached to the TEMs. Dose rates used were $0.8\text{--}3.1 \times 10^{24}$ e/m²s. Irradiation was carried out at 298 K (75 keV and 200 keV), 100 K (200 keV), and 90 K (75 keV). All the TEM images and selected area electron diffraction (SAED) patterns were recorded using CCD cameras (Gatan Orius200 and UltraScan1000) or a CMOS camera (Gatan OneView). Compositional analysis was performed in scanning mode (STEM) using an energy-dispersive x-ray spectrometer (EDS, JEOL JED-2300) attached to the 200 kV-TEM. Specimen thickness was estimated by electron energy-loss spectroscopy with the log-ratio method.

3. Results

3.1. Plan-view TEM observations

3.1.1. Electron irradiation (75 keV) of a freestanding a-Pd-Si alloy thin films

Fig. 1(a) shows a selected area electron diffraction (SAED) pattern of an as-deposited, freestanding a-Pd-Si alloy film. We used a relatively thick film (~ 100 nm) to reduce an effect of possible surface oxidation of the freestanding Pd-Si film. A halo pattern indicates the presence of amorphous phase. The first halo peak is located at 4.45 nm^{-1} and is almost comparable to the value reported in the literature [15] (scattering vector *q* is defined as $q = 2\sin\theta / \lambda$). Fig. 1(b) shows an SAED pattern of the specimen after the 75 keV-electron irradiation at 298 K for 2.9 ks (total dose: 2.9×10^{27} e/m²). The halo pattern changed to a diffuse Debye-Scherrer rings. The pattern can be indexed by face-centered cubic (fcc) structure. This result indicates an early stage of crystallization induced by electron irradiation. Actually, in the initial stage of thermal crystallization of the a-Pd₈₀Si₂₀ alloy, appearance of a number of small Pd crystallites with a fcc structure was reported in the literature [10]. However, it should be emphasized here that the change observed in the SAED in Fig. 1 is completely different from those observed in the a-SiO_x/a-Pd-Si/a-SiO_x composite films shown later in Figs. 2-4. Also note that under 75 keV-electron irradiation, knock on atom displacement is excluded both for Pd and Si [16]. Although the clarification of the cause of the change in the SAED seems interesting, it will be out of the scope of the present study. Similar results were also obtained with 200 keV-electron irradiation (see Fig.S1 in the supplementary materials).

3.1.2. Electron irradiation (75 keV) of a-SiO_x/a-Pd-Si/a-SiO_x composite thin films

Fig. 2(a) and 2(b) show a bright-field (BF) TEM image and the corresponding SAED pattern of an as-deposited a-SiO_x/a-Pd-Si/a-SiO_x composite thin film, respectively. The total thickness of the composite film is ~ 40 nm. Granular microstructure with a rather uniform contrast is seen in the BF-TEM image. A halo pattern indicates the formation of amorphous phase of Pd-Si as well as the presence of a-SiO_x. After 75 keV-electron irradiation at 298 K for 900 s (total dose: 2.7×10^{27} e/m²), extensive coalescence and growth of the microstructure (namely, grain growth) occurred as shown in Fig. 2(c). A halo pattern of the as-deposited specimen changed to sharp, but discontinuous Debye-Scherrer rings (Fig. 2(d)). The crystallized phase was judged to be hexagonal Pd₂Si (Fe₂P-type structure, $P\bar{6}2m$) [17,18] based on the analysis of SAED patterns (detailed indexing are shown in Fig. 3). This phase is identical to that reported in the preceding study on a-(Pd-Si)/SiO_x [11], but differs from the phase reported for annealed Pd₈₀Si₂₀ amorphous alloy ribbon where orthorhombic Pd₃Si is the stable phase [10]. It is emphasized here that the crystallization behavior of the composite film essentially differs from that observed in the freestanding a-Pd-Si film. Namely, a notable feature is that the crystallization process is completely different between the composite and free-standing films,

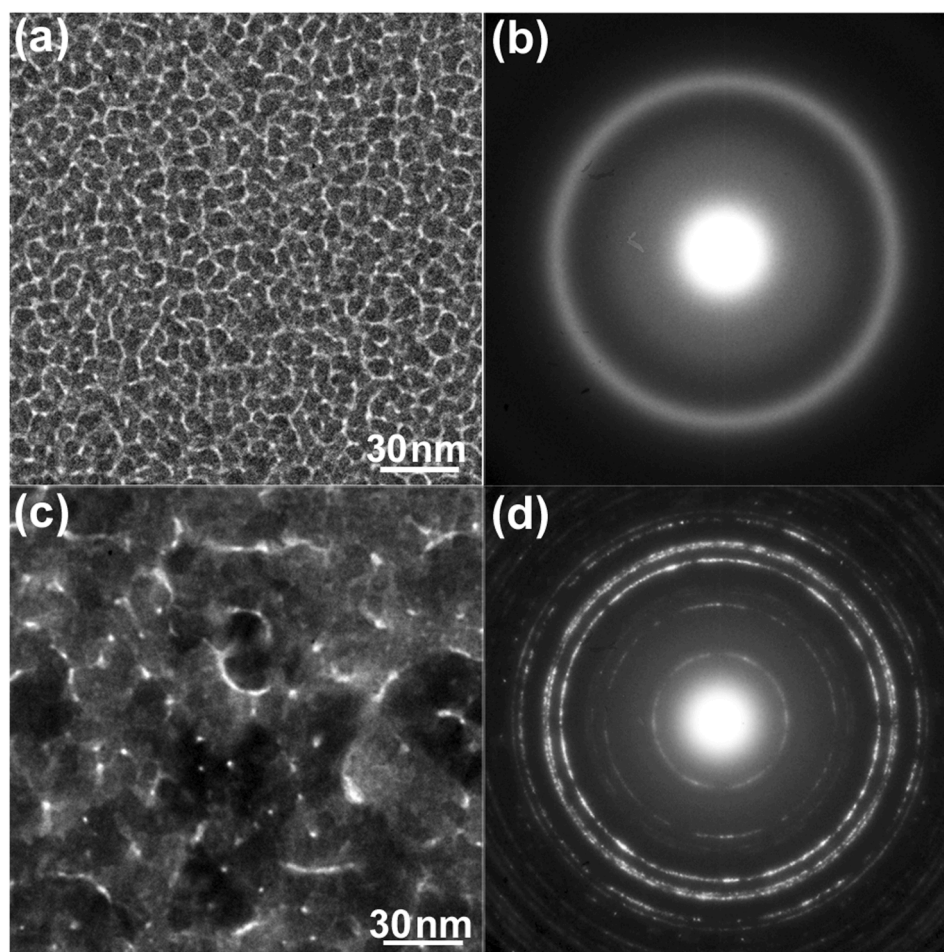


Fig. 2. BF-TEM images and corresponding SAED patterns of an a-SiO_x/a-Pd-Si/a-SiO_x composite thin film. (a, b) as-deposited, (c, d) after 75 keV-electron irradiation at 298 K for 900 s (total dose: 2.7×10^{27} e/m²).

both in terms of crystallization rate and the resulting crystalline phase, as can be seen from the changes in the SAED patterns (i.e. compare Fig. 1 (b) with 2(d)). Effect of a-SiO_x films on the crystallization of a-Pd-Si will be discussed later.

Fig. 3(a) shows electron diffraction intensity profiles of the as-deposited and the 75 keV-electron irradiated specimens. The intensities were integrated in the circumference direction in each diffraction pattern. After electron irradiation, crystallization can be recognized as appearance of sharp diffraction peaks such as $\bar{1}2\bar{1}1$ and $\bar{1}3\bar{2}0$. A part of the SAED pattern after irradiation for 900 s is shown in Fig. 3(b) with Miller indices. In this pattern, absence of a halo ring, for example, one near the 02 $\bar{2}$ 1 Debye ring, indicates that a rather complete crystallization was induced by the irradiation.

Fig. 4(a) and 4(b) show a BF-TEM image and the corresponding SAED pattern of an as-deposited a-SiO_x/a-Pd-Si/a-SiO_x composite thin film observed at 90 K, respectively. Fig. 4(c) and 4(d) show those after 75 keV electron irradiation at 90 K for 900 s (total dose: 2.7×10^{27} e/m²), respectively. Certainly, coalescence and growth of the microstructure occurred also at this reduced temperature, as shown in Fig. 4 (c), and Debye-Scherrer rings indicate similarly formation of the hexagonal Pd₂Si phase (Fig. 4(d)). Although irradiation condition except temperature was the same as that employed at 298 K in the experiments shown in Fig. 4, granular microstructure remains albeit the grain growth and hence the Debye-Scherrer rings are continuous. This is in sharp contrast to the very rapid grain growth at 298 K (Fig. 2(c)) where Debye-Scherrer rings became discontinuous (Fig. 2(d)). This fact that grain growth at 298 K is very rapid as compared with that at 90 K may suggest

that the migration rate of Pd and Si for the Pd₂Si compound formation depend on temperature in a natural manner. Anyway, it can be concluded that crystallization by electronic excitation is realized by 75 keV irradiation at 90 K at a somewhat reduced rate as compared to the irradiation at 298 K.

Finally, it is noted at the end of Section 3.1. that the hexagonal Pd₂Si phase was also obtained by 200 keV-electron irradiation in the a-SiO_x/a-Pd-Si/a-SiO_x composite thin films both at 298 K (Fig. S2) and 100 K (Fig. S4). The overall feature obtained are essentially the same as those obtained for 75 keV-electron irradiation described above. Microstructural coalescence and growth during crystallization were more pronounced with 75 keV irradiation than with 200 keV irradiation. This is because as the electron energy decreases, the ionization cross section of the core electron increases [19]. Experimental results obtained by 200 keV irradiation are shown in Figs.S2-S4 in the supplementary materials. Under 200 keV-electron irradiation, knock-on atom displacement of Pd is excluded, while that of Si may be involved [16]. However, possible contribution of knock-on atom displacement to atomic migration must be limited since the Pd content exceeds 80% in our specimen.

3.2. Cross-sectional TEM observation

Fig. 5(a) shows a cross-sectional TEM image of the as-deposited a-SiO_x/a-Pd-Si/a-SiO_x composite thin film. As seen, a-Pd-Si layer with thickness of 22 nm is sandwiched between the a-SiO_x layers. The a-Pd-Si layer containing heavy Pd shows darker contrast compared to the a-SiO_x layer. The interface between a-Pd-Si and a-SiO_x is not flat and

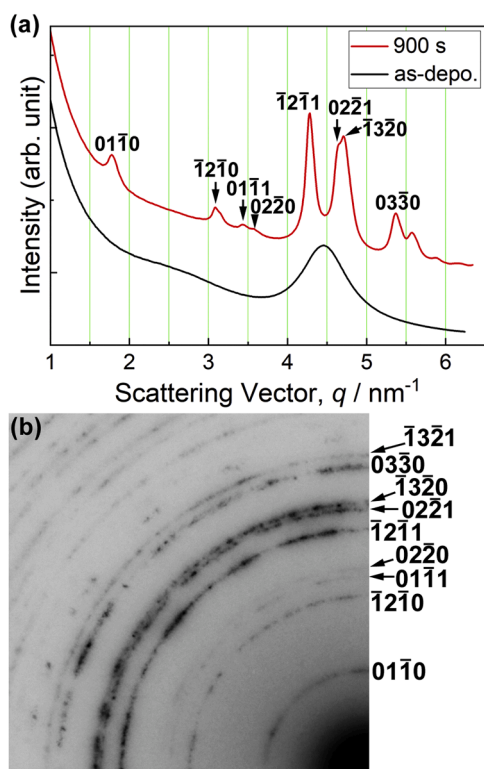


Fig. 3. (a) Electron diffraction intensity profiles of the as-deposited and the 75 keV-electron irradiated a-SiO_x/a-Pd-Si/a-SiO_x composite thin film. (b) A part of the SAED pattern after electron irradiation at 298 K for 900 s.

nanometer-scale roughness is seen. Lower inset shows the SAED pattern. Strong diffraction spots come from the Si(111) substrate (not shown here). Very weak halo rings indicate amorphous phase of the composite thin film. Fig. 5(b) shows a cross-sectional TEM image of the composite thin film after 200 keV-electron irradiation at 298 K (total dose: 5.0×10^{26} e/m²). Lattice fringes of ~ 0.24 nm spacing are seen in the Pd-Si layer, which can be attributed to the ($\bar{1}2\bar{1}1$) atomic planes of the hexagonal Pd₂Si. A Debye-Scherrer ring marked by an arrowhead in the attached SAED pattern is $\bar{1}2\bar{1}1$ of the Pd₂Si. According to the EDS analysis, chemical composition of the central part of the Pd-Si layer was Pd-31at%Si, which is close to the Pd₂Si. Note that Si concentration increased due to the compound formation (initial alloy composition was Pd-19at%Si). Thus, cross-sectional TEM observation also revealed that the a-Pd-Si layer was crystallized to hexagonal Pd₂Si by 200 keV-electron irradiation. Noticeable feature here is that thickness of the Pd-Si layer increased by ~ 3 nm after crystallization, while the volume reduction should occur by crystallization in general.

Fig. 6(a) shows a cross-sectional BF-STEM image observed at the interface between the irradiated and as-deposited area. Pd-Si layer is imaged as dark contrast sandwiched by a-SiO_x layers with gray contrast. As seen, it is obvious that the Pd-Si layer thickness of the irradiated region is thicker than that of the non-irradiated region. Fig. 6(b) shows a HAADF-STEM image obtained from the same area shown in Fig. 6(a). The spread of the Pd-Si layer is clearly observed with bright contrast (atomic number contrast), especially along the bottom left of the a-Pd-Si layer.

4. Discussion

Experimental results can be summarized as follows.

- (1) Crystallization of Pd-19at%Si amorphous alloy in an a-SiO_x/a-Pd-Si/a-SiO_x composite film occurs by 75 keV and 200 keV electron irradiation even below room temperature.
- (2) A resultant product of the crystallization after electron irradiation (hexagonal Pd₂Si) differs from that of thermal annealing (orthorhombic Pd₃Si).

Based upon the results, the following mechanism is proposed for the crystallization.

4.1. Crystallization mechanism during electron irradiation

Decomposition of a-SiO_x occurs via electronic excitation induced by electron irradiation (75 and 200 keV). This process involves inner-shell electron excitation; Auger decay of the core hole is responsible for the decomposition of a-SiO_x [12,13]. In our previous photon irradiation experiments (photon energy of 80–680 eV), we found that the excitation of Si2p electrons (binding energy of ~ 100 eV) is essential for the decomposition of a-SiO_x [12]. In contrast, it should be noted that 75 keV-electrons can excite all core electrons including the ground state. One of the dissociation products (i.e., free Si) is highly reactive and hence it immediately forms a chemical bond with an adjacent atom or simply return to the original state (a-SiO_x). Decomposition of a-SiO_x by electronic excitation contributes essentially to the crystallization of a-Pd-Si in the composite film, since the structural change of the free-standing a-Pd-Si film due to a similar electron irradiation is remarkably small in degree and different in nature. If dissociated Si atoms dissolve into the a-Pd-Si layer across the a-Pd-Si/a-SiO_x interface, then composition of the a-Pd-Si layer (initially Pd-19at%Si) shifts towards high Si content. In fact, a composition of Pd-31at%Si was obtained in the central part of the Pd-Si layer after electron irradiation. In our previous study on Pt/a-SiO_x system [12], it was found that composition of the a-SiO_x ($x \sim 1.5$) shifts towards stable SiO₂ with the formation of Pt₂Si (this can be confirmed by the shift of the first halo ring position of a-SiO_x). It should be mentioned that the amount of Si atoms necessary for the Pd₂Si formation from Pd-19at%Si is one third of those required for the Pt₂Si formation from pure Pt. The a-Pd-Si layer is sandwiched between a-SiO_x layers, and when a part of the a-SiO_x is dissociated by electronic excitation, then chemically active Si atoms can be alloyed with the a-Pd-Si layer across the interface.

Fig. 7(a) shows a schematic of Pd₂Si formation at the a-Pd-Si/a-SiO_x interface by electron irradiation. Electronic excitation first breaks a Si–O bond, which is immediately followed by alloying of dissociated Si with a-Pd-Si at the interfaces, and eventually leads to the crystalline Pd₂Si formation. However, energy transfer due to nonradiative relaxation after electronic excitation would not enough for atoms to migrate in a long distance. To sustain the crystallization, it is necessary to supply Si to the reaction front on the surface of the previously formed Pd₂Si crystallite that exists between an amorphous Pd-Si and an a-SiO_x layer. One method of achieving such a supply is an extensive morphology change of the grains, which would facilitate a steady and constant supply of active reaction front. Morphology change observed in Fig. 2(c) (298 K) and 4(c) (90 K) may correspond to such a situation. A prominent morphology change was observed even at 90 K in the case of α -Pt₂Si formation at Pt/a-SiO_x interface [20]. It should be noted that pure Si nanoclusters which can be detected by TEM are not formed in our study [12], unlike previous electron irradiation studies using huge energy electrons (20 MeV) [21] or highly intense electron beam (6.2×10^{27} e/m²) [22].

Based on the above considerations, it is reasonable to interpret that the observed slight increase of the a-Pd-Si layer thickness after electron irradiation (Fig. 5(b)) can be attributed to a Si supply to the a-Pd-Si layer induced by dissociation of a-SiO_x. Once the alloy composition reaches ~ 33 at%Si, then crystallization would start immediately since the Pd₂Si is the thermodynamically stable line compound with a remarkably high melting temperature (1604 K) [23] and a large heat of formation ($\Delta H =$

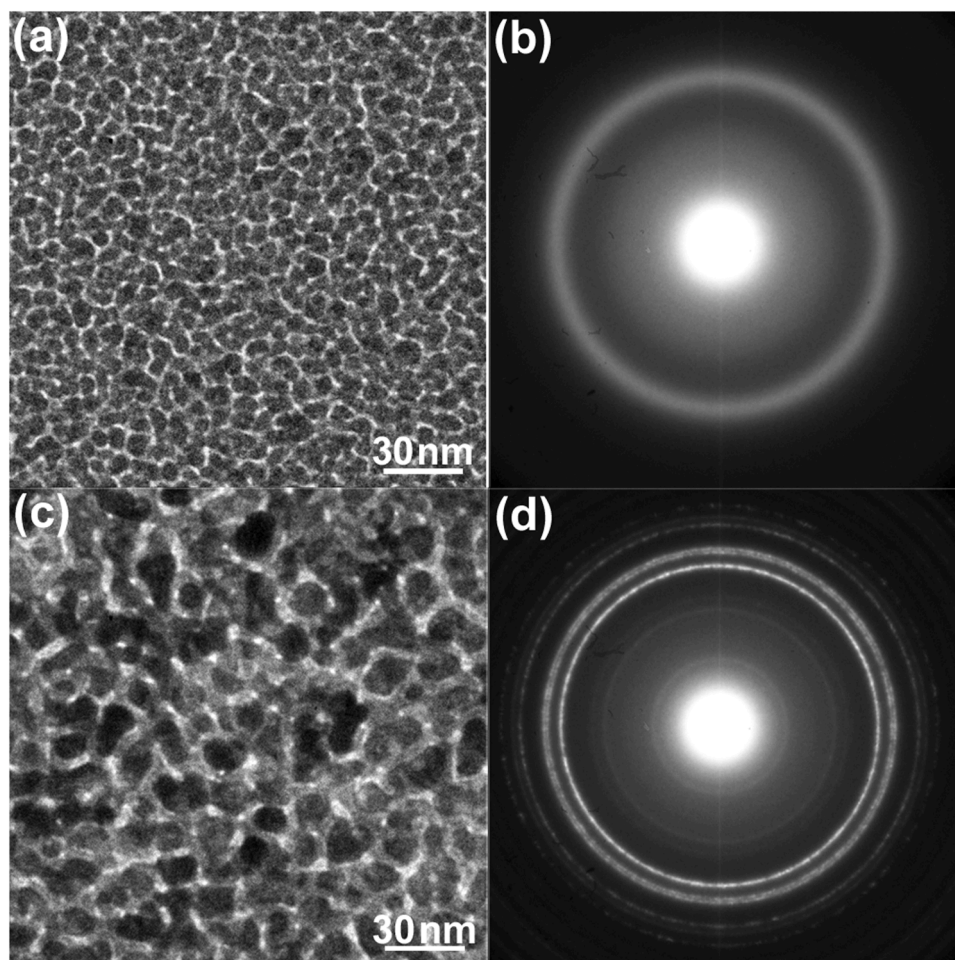


Fig. 4. BF-TEM images and corresponding SAED patterns of an a-SiO_x/a-Pd-Si/a-SiO_x composite thin film observed at 90 K. (a, b) as-deposited, (c, d) after 75 keV-electron irradiation for 900 s (total dose: 2.7×10^{27} e/m²).

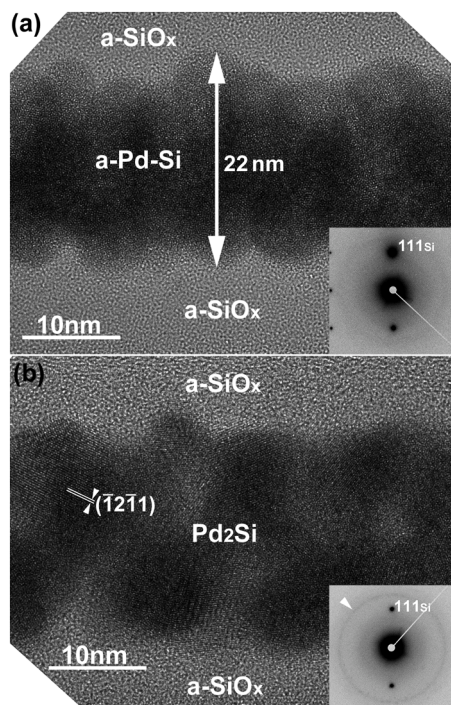


Fig. 5. Cross-sectional TEM images of an a-SiO_x/a-Pd-Si/a-SiO_x composite film. (a) as-deposited, (b) after 200 keV-electron irradiation at 298 K with the total dose of 5.0×10^{26} e/m².

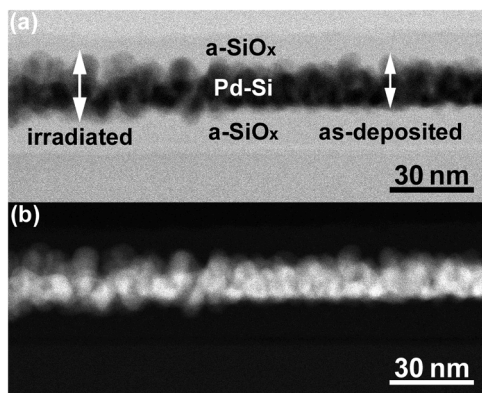


Fig. 6. Cross-sectional STEM images observed at the interface between the irradiated and as-deposited area. (a) BF-STEM image, (b) HAADF-STEM image.

–43 kJ/mol) [24] as shown in Fig. 7(b) (location of the Pd₂Si phase is indicated by a vertical green line) [23]. The liquidus draws a sharp convex parabolic shape with the vertex at 33at%Si, in contrast to the eutectic composition that forms a deep valley around 17at%Si. It is presumed that supply of Si atoms to the a-Pd-19at%Si layer causes instability of the amorphous phase; i.e., additional solute atom mediated crystallization, which is a new mechanism of crystallization of amorphous alloy. This reminds us of the crystallization of amorphous nanoparticles by spontaneous alloying: where vapor deposition of Au onto amorphous antimony nanoparticles rapidly formed AuSb₂ compounds at room temperature [25].

5. Conclusions

Electron irradiation induced crystallization of Pd-19at%Si amorphous alloy thin films have been studied by TEM and electron diffraction. Crystallization of Pd-19at%Si amorphous phase in an a-SiO_x/a-Pd-

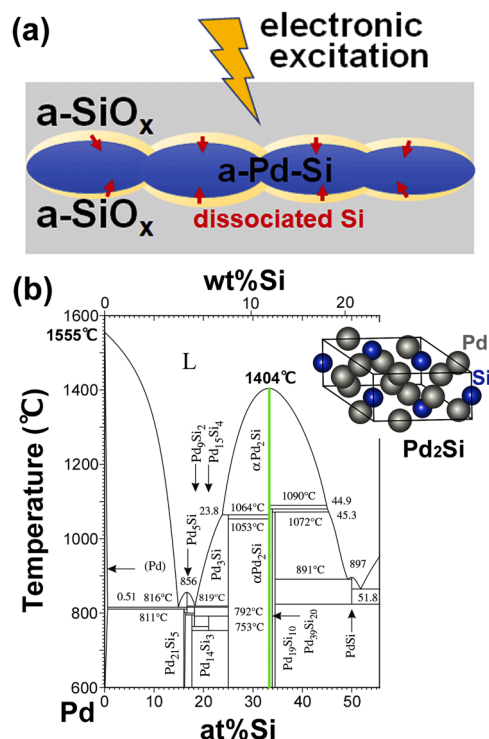


Fig. 7. (a) Schematic illustration of dissolution of naked Si atoms into a-Pd-Si layer induced by dissociation of a-SiO_x under electron irradiation. Electronic excitation first breaks a Si–O bond, which is immediately followed by alloying of the dissociated Si with a-Pd-Si at the interfaces (pale yellow region), and eventually, leads to the Pd₂Si formation. (b) Equilibrium phase diagram of the Pd-Si system [23].

Si/a-SiO_x composite film occurred by 75 keV and 200 keV electron irradiation below room temperature. A resultant product of the crystallization after electron irradiation is the hexagonal Pd₂Si, which differs from that after thermal annealing (orthorhombic Pd₃Si). We concluded that crystallization by electronic excitation is realized, at least, by 75 keV electron irradiation at 90 K. Decomposition of a-SiO_x by electronic excitation contributes essentially to the crystallization of the a-Pd-Si in the composite film, since the structural change of the free standing a-Pd-Si film due to a similar electron irradiation is remarkably small in degree and different in nature. It is presumed that the supply of dissociated Si (naked Si) to the a-Pd-Si layer causes instability of the amorphous phase, which is the trigger for the remarkable structural change; i.e., crystalline Pd₂Si formation. We propose a new mechanism of crystallization of amorphous alloy mediated by additional solute atoms produced by electronic excitation. Further study is needed to make clear the atomic process of Si injection into a-Pd-Si alloy followed by crystallization.

Declaration of Competing Interest

The authors declare no competing interest.

Acknowledgments

The authors wish to thank Mr. D. Furukawa and Dr. S. Takagi for their helps in this study. This study was partially supported by the program Advanced Research Network for Ultra-Microscopic Science (FY2016–2021) from the Ministry of Education, Culture, Sports, Science, and Technology (MEXT), Japan and the JSPS KAKENHI grant no. 21H01764 and no. 20K21129.

Supplementary materials

Supplementary material associated with this article can be found, in the online version, at [doi:10.1016/j.mta.2023.101888](https://doi.org/10.1016/j.mta.2023.101888).

References

- [1] S.R. Elliot, *Physics of Amorphous Materials*, 2nd ed., John Wiley & Sons, Inc. NY, 1990.
- [2] T. Masumoto, H. Kimura, A. Inoue, Y. Waseda, Structural stability of amorphous alloys, *Mater. Sci. Eng.* 23 (1976) 141–144.
- [3] W.L. Johnson, A. Inoue, C.T. Liu, *Bulk Metallic Glasses*, Materials Research Society, Warrendale, 1999.
- [4] A. Meldrum, L.A. Boatner, R.C. Ewing, Electron-irradiation-induced nucleation and growth in amorphous LaPO₄, ScPO₄, and zircon, *J. Mater. Res.* 12 (1997) 1816–1827.
- [5] R. Nakamura, M. Ishimaru, H. Yasuda, H. Nakajima, Atomic rearrangements in amorphous Al₂O₃ under electron-beam irradiation, *J. Appl. Phys.* 113 (2013), 064312.
- [6] I. Jencić, I.M. Robertson, J. Skvarč, Electron beam induced regrowth of ion implantation damage in Si and Ge, *Nucl. Inst. Met. Phys. Res. B* 148 (1999) 345–349.
- [7] M. Okugawa, R. Nakamura, M. Ishimaru, K. Watanabe, H. Yasuda, H. Numakura, Structural transition in sputter-deposited amorphous germanium films by aging at ambient temperature, *J. Appl. Phys.* 119 (2016), 214309.
- [8] M. Okugawa, R. Nakamura, H. Numakura, M. Ishimaru, H. Yasuda, Dual crystallization modes of sputter-deposited amorphous SiGe films, *J. Appl. Phys.* 128 (2020), 015303.
- [9] P. Duwez, R.H. Willens, R.C. Crewdson, Amorphous phase in palladium-silicon alloys, *J. Appl. Phys.* 36 (1965) 2267–2269.
- [10] T. Masumoto, R. Maddin, The mechanical properties of palladium 20a/o silicon alloy quenched from the liquid state, *Acta Met.* 19 (1971) 725–741.
- [11] T. Nagase, R. Yamashita, J.-G. Lee, Electron-irradiation-induced crystallization at metallic amorphous/silicon oxide interface caused by electronic excitation, *J. Appl. Phys.* 119 (2016), 165103.
- [12] K. Sato, H. Yasuda, S. Ichikawa, M. Imamura, K. Takahashi, S. Hata, S. Matsumura, S. Anada, J.-G. Lee, H. Mori, Synthesis of platinum silicide at platinum/silicon oxide interface by photon irradiation, *Acta Mater.* 154 (2018) 284–294.
- [13] H. Yasuda, K. Sato, S. Ichikawa, M. Imamura, K. Takahashi, H. Mori, Promotion in solid phase reaction of Pt/SiO_x bilayer film by electron-orbital-selective-excitation, *RSC Adv.* 11 (2021) 894–898.
- [14] J.-G. Lee, T. Nagase, H. Yasuda, H. Mori, Synthesis of metal silicide at metal/silicon oxide interface by electronic excitation, *J. Appl. Phys.* 117 (2015), 194307.
- [15] M. Matsushita, Y. Hirotsu, K. Anazawa, T. Ohkubo, T. Oikawa, Electron diffraction intensity analysis of amorphous alloy thin film with imaging-plate technique, *Mater. Trans. JIM* 36 (1995) 822–827.
- [16] K. Urban, Radiation-induced processes in experiments carried out in-situ in the high-voltage electron microscope, *Phys. Stat. Sol. (a)* 56 (1979) 157–168.
- [17] P. Villars, *Pearson's Handbook: Desk Edition: Crystallographic Data For Intermetallic Phases*, ASM International, OH, 1998.
- [18] Y. Hirotsu, T. Ohkubo, M. Matsushita, Study of amorphous alloy structures with medium range atomic ordering, *Microsc. Res. Tech.* 40 (1998) 284–312.
- [19] C.J. Powell, Cross-sections for ionization of inner-shell electrons by electrons, *Rev. Mod. Phys.* 48 (1976) 33–47.
- [20] K. Sato, H. Mori, Athermal solid phase reaction in Pt/SiO_x thin films induced by electron irradiation, *ACS Omega* 6 (2021) 21837–21841.
- [21] T. Hristova-Vasileva, P. Petrik, D. Nesheva, Z. Fogarassy, J. Lábár, S. Kaschieva, S. N. Dmitriev, K. Antonova, Influence of 20 MeV electron irradiation on the optical properties and phase composition of SiOx thin films, *J. Appl. Phys.* 123 (2018), 195303.
- [22] G.S. Chen, C.B. Boothroyd, C.J. Humphreys, Electron-beam-induced damage in amorphous SiO₂ and the direct fabrication of silicon nanostructures, *Phil. Mag. A* 78 (1998) 491–506.
- [23] H.C. Baxi, T.B. Massalski, The Pd-Si (Palladium-Silicon) system, *J. Phase Equilibria* 12 (1991) 349–356.
- [24] R. Pretorius, T.K. Marais, C.C. Theron, Thin film compound phase formation sequence: an effective heat of formation model, *Mat. Sci. Eng.* 10 (1993) 1–83.
- [25] H. Mori, H. Yasuda, Formation of AuSb₂ compound clusters by spontaneous alloying, *Intermetallics* 1 (1993) 35–40.